Electronic Supplementary Material (ESI) for Journal of Materials Chemistry C.

Influence of the Electronic Structures of Diketopyrrolopyrrole-based Donor-Acceptor Conjugated Polymers on Thermoelectric Performance

Sang Beom Kim,‡[a] Seunghoon Song, ‡[b] Taek Seong Lee,[a] Muhammad Kiki Afindia Joenata,[b] Eui Hyun Suh,[c] Yong Jin Jeong,[d,] Jaeyoung Jang,[a,*] Yun-Hi Kim[b,*]*

[a] Department of Energy Engineering, Hanyang University, Seoul 04763, Republic of Korea.

[b] Department of Chemistry and Research Institute Molecular Alchemy (RIMA), Gyeongsang National University, Jinju, 52828, Republic of Korea

[c] Department of Chemical and Environmental Engineering, University of Arizona, Tucson, Arizona 85721, United States

[d] Department of Materials Science and Engineering, Korea National University of Transportation, Chungju 27469, Republic of Korea.

Experimental Section

Materials

All the chemicals were purchased from Aldrich, TCI, and Alfa Chemical Co. Dimethyl succinate, 11-(bromomethyl)tricosane, NBS, n-BuLi, and 2-thiophenecarbonitrile were used as received without further purification. All the solvents were purified prior to use. 3,6-Bis(5-bromothiophen-2-yl)-2,5-bis(7-decylnonadecyl)-2,5-dihydropyrrolo[3,4-c]pyrrole-1,4-dione, (*E*)-1,2-bis(5-(trimethylstannyl)thiophen-2-yl)ethene, and (*E*)-2,3-bis(5-(trimethylstannyl)thiophen-2-yl)acrylonitrile were obtained using a previously published method.[1-3]

Synthesis of CN1. The polymer was synthesized via Stille coupling using a palladium catalyst. 3,6-bis(5-bromothiophen-2-yl)-2,5-bis(7-decylnonadecyl)pyrrolo[3,4-c]pyrrole-1,4(2*H*,5*H*)-dione (0.200 g, 0.157 mmol), (*E*)-2,3-bis(5-(trimethylstannyl)thiophen-2-yl)acrylonitrile (0.0085 g, 0.016 mmol), and (*E*)-1,2-bis(5-(trimethylstannyl)thiophen-2-yl)ethene (0.073 g, 0.142 mmol) were dissolved in dry chlorobenzene (10 mL) in a Schlenk flask. After degassing under nitrogen for 30 min, $Pd_2(dba)_3$ (1.44 mg) and P(*o*-Tol)$_3$ (1.91 mg) were added to the mixture, which was then stirred for 3 h at 85 °C. After 3 h, 2-bromothiophene and tributyl(thiophen-2-yl)stannane were added to the reaction mixture for end-capping. After the polymer was precipitated in methanol, it was collected by filtration and successively purified using Soxhlet extraction with methanol, acetone, hexane, and toluene. The final product, poly[2,5-bis(7-decylnonadecyl)pyrrolo[3,4-c]pyrrole-1,4(2H,5H)-dione-(E)-2,3-di(thiophen-2-yl)acrylonitrile-co-[2,5bis(7-decylnonadecyl)pyrrolo[3,4-c]pyrrole-1,4(2H,5H)-dione-(E)-1,2-di(thiophen-2-yl)ethene (CN1), was obtained by precipitation in methanol. Yield: 0.16 g, ^{1}H NMR (300MHz, $CDCl_3$) δ = 8.92 (br, 4H), 6.64-6.38 (br, 6H), 4.84-4.77 (br, 4H), 1.94-1.00 (br, 102H) 0.87-0.79 (br, 12H), (Mn = 982000, Mw = 1032000, PDI = 1.05).

Synthesis of CN3. The polymer was synthesized via Stille coupling using a palladium catalyst following the CN1 synthesis process. CN3 was obtained via precipitation in methanol. Yield: 0.21 g, ^{1}H NMR (300MHz, $CDCl_3$) δ = 8.91-8.90 (br, 4H), 6.84 (br, 6H), 4.67-4.65 (br, 4H), 1.50-1.00 (br, 102H) 0.83-0.70 (br, 12H), (Mn = 1287000, Mw = 1406000, PDI = 1.09).

Synthesis of CN5. The polymer was synthesized via Stille coupling using a palladium catalyst following the CN1 synthesis process. CN5 was obtained via precipitation in methanol. Yield: 0.11 g, ^{1}H NMR (300MHz, $CDCl_3$) δ = 8.90-8.89 (br, 4H), 6.84 (br, 6H), 5.42-3.3 (br, 4H), 1.47-1.18 (br, 102H) 0.86-0.73 (br, 12H), (Mn = 1105000, Mw = 1302000, PDI = 1.18).

Synthesis of CN7. The polymer was synthesized via Stille coupling using a palladium catalyst following the CN1 synthesis process. CN7 was obtained via precipitation in methanol. Yield: 0.18 g, ^{1}H NMR (300MHz, $CDCl_3$) δ = 8.93-8.73 (br, 4H), 6.84 (br, 6H), 5.11-3.91 (br, 4H), 1.47-1.12(br, 102H) 0.84-0.70 (br, 12H), (Mn =1213000, Mw = 1332000, PDI = 1.10).

Synthesis of CN9. The polymer was synthesized via Stille coupling using a palladium catalyst following the CN1 synthesis process. CN9 was obtained via precipitation in methanol. Yield: 0.21 g, ^{1}H NMR (300MHz, $CDCl_3$) δ = 8.90 (br, 4H), 6.84-6.73 (br, 6H), 3.98-3.94 (br, 4H), 1.34-1.02 (br, 102H) 0.84-0.72 (br, 12H), (Mn = 748000, Mw = 1282000, PDI = 1.71).

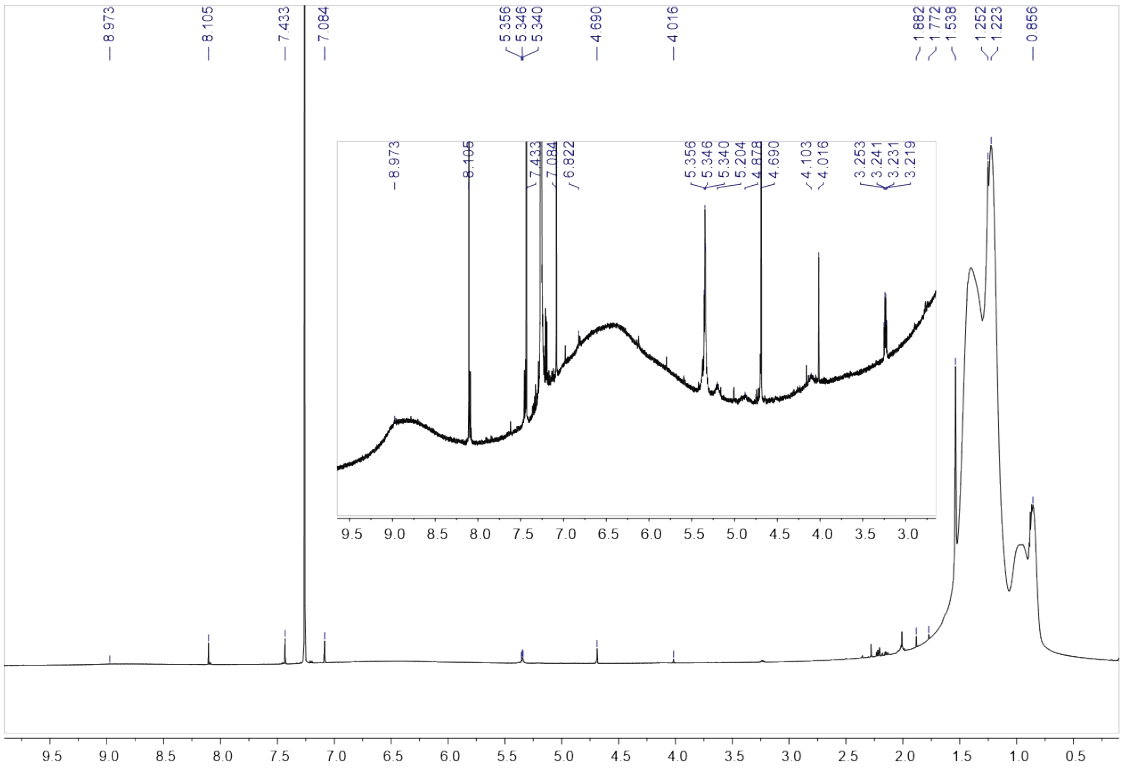

Fig. S1. ^{1}H Nuclear magnetic resonance (NMR) spectrum of CN1. ($CDCl_3$, 600 MHz)

Fig. S2. ^{1}H NMR spectrum of CN3. ($CDCl_3$, 600 MHz)

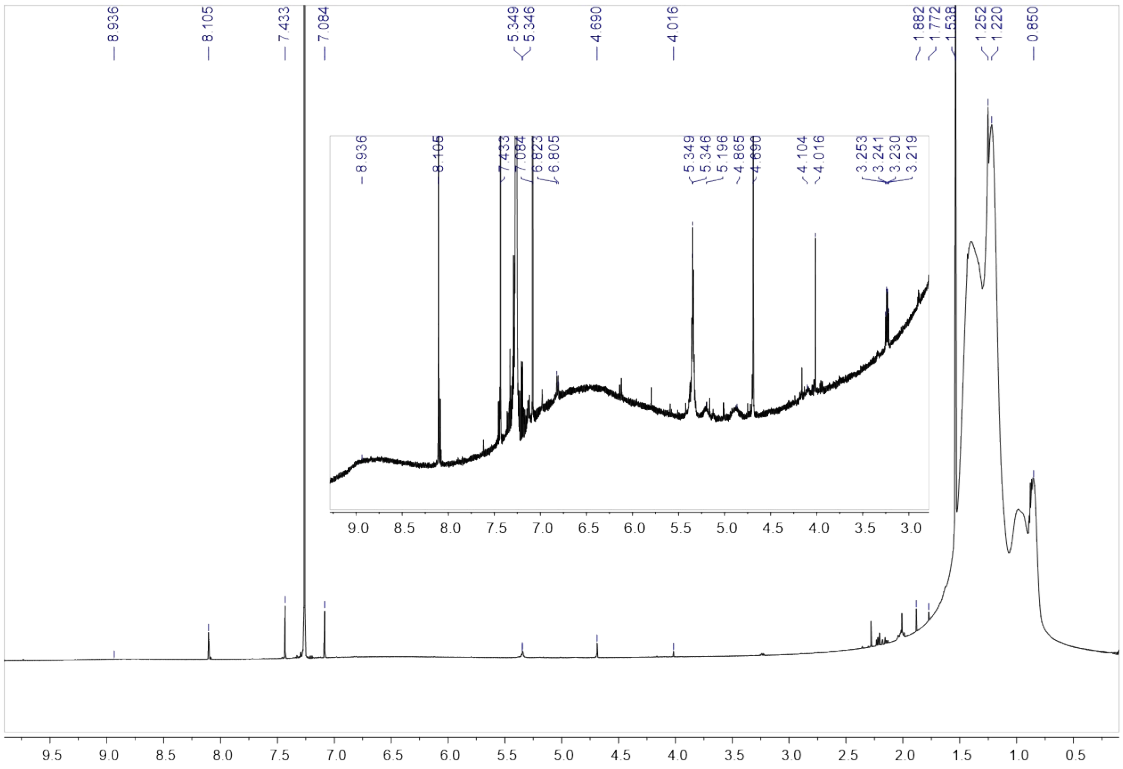

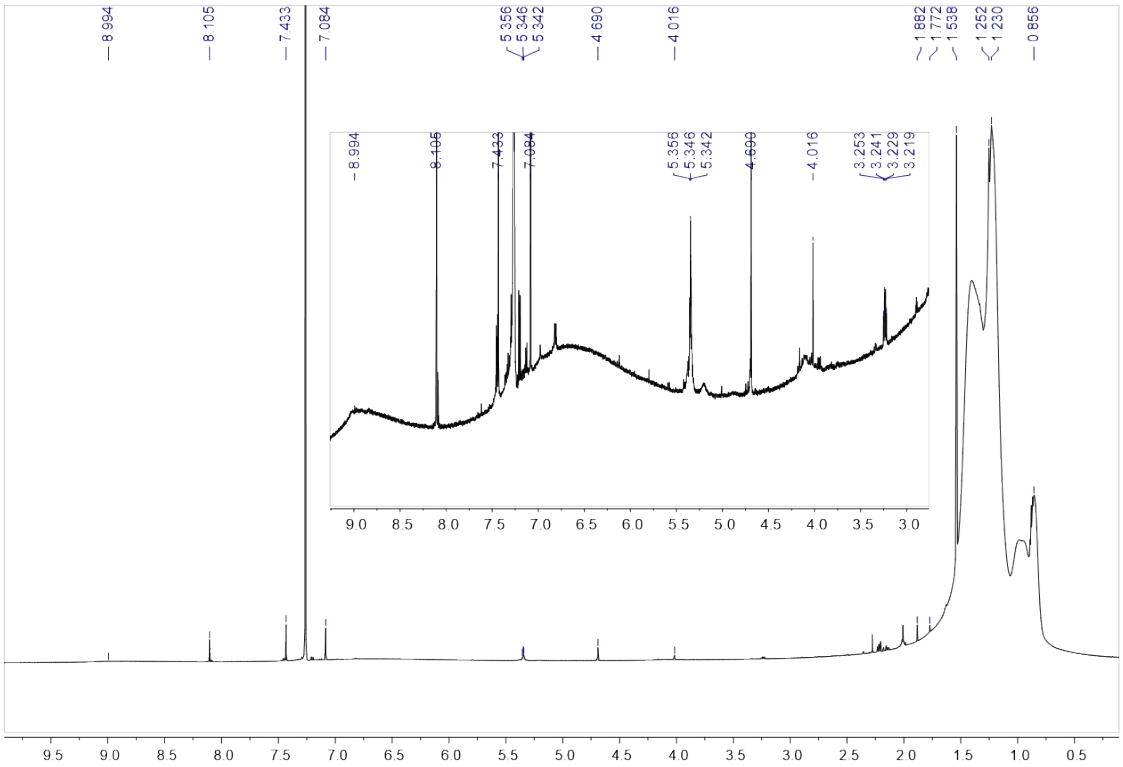

Fig. S3. ^{1}H NMR spectrum of CN5. ($CDCl_3$, 600 MHz)

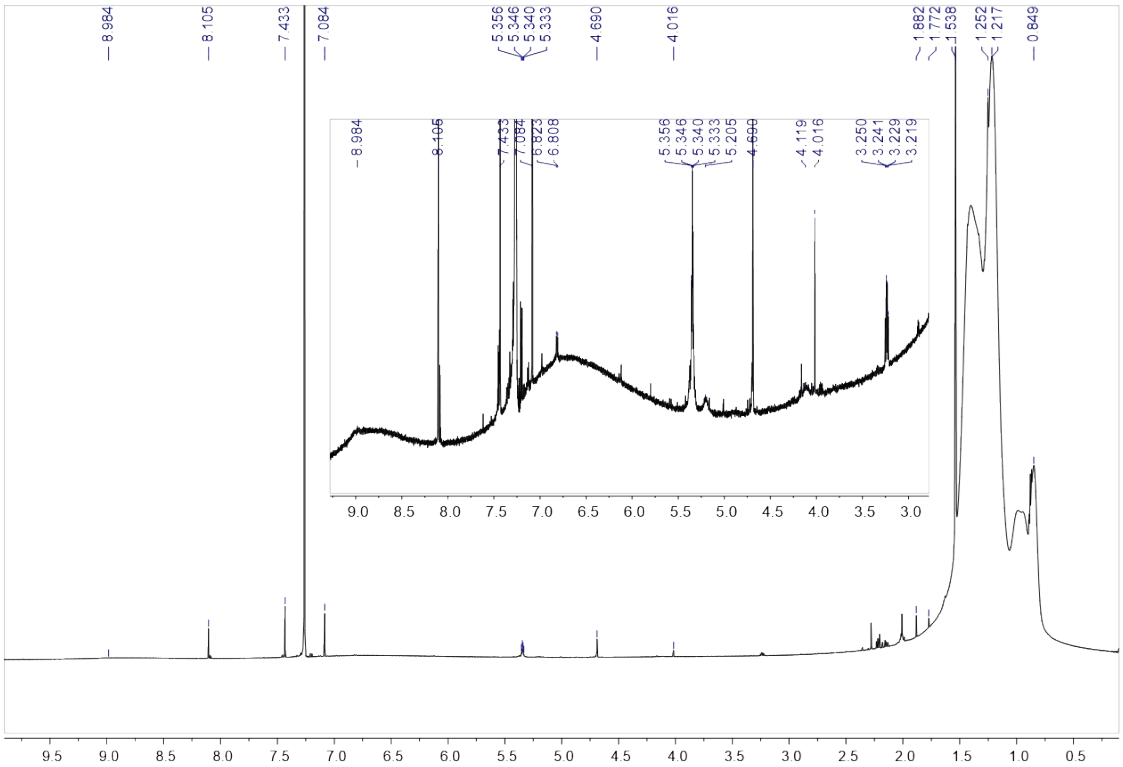

Fig. S4. ^{1}H NMR spectrum of CN7. ($CDCl_3$, 600 MHz)

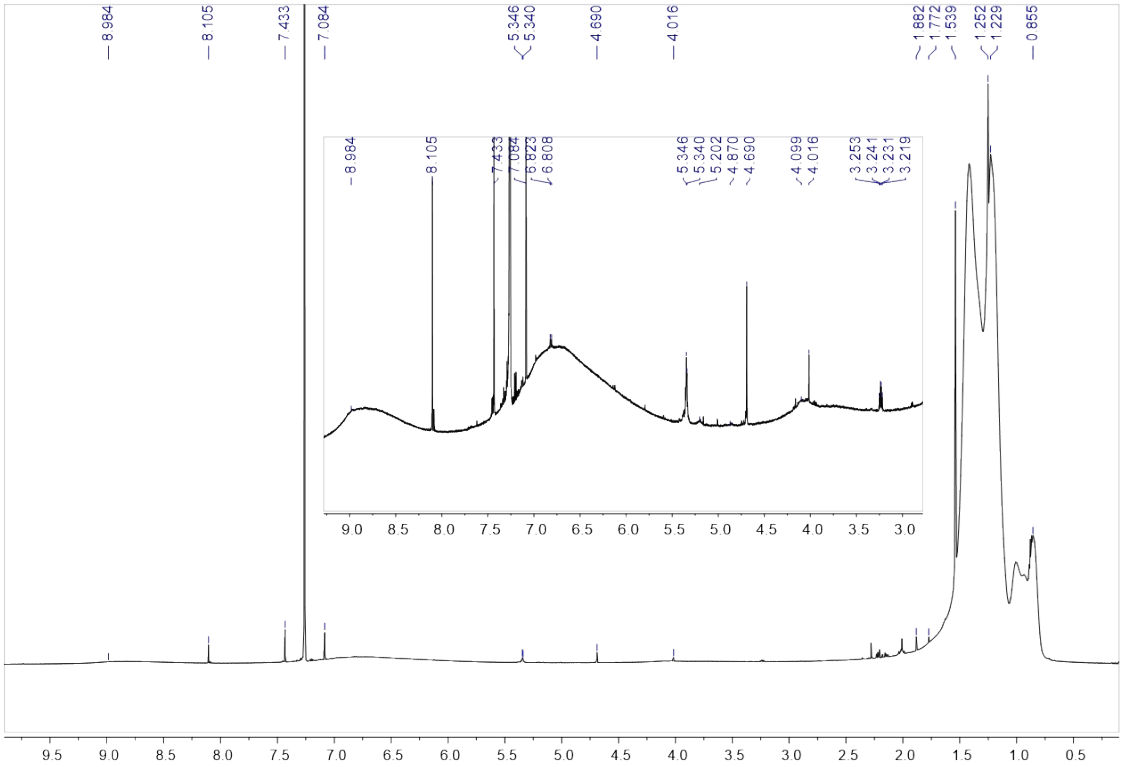

Fig. S5. ^{1}H NMR spectrum of CN9. ($CDCl_3$, 600 MHz)

CN1

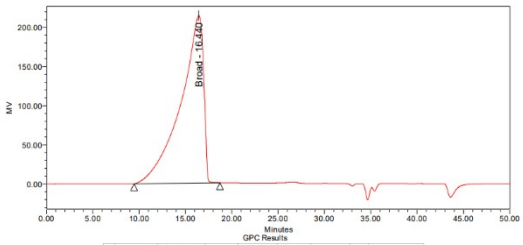

	Dist Name	Retention Time (min)	% Area	% Height	Mn	Mw	MP	Polydispersity
1		16.440	100.00	100.00	982134	1032182		1.050959

CN3

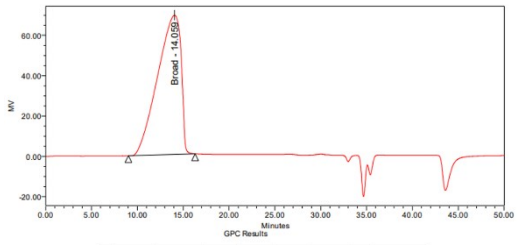

	Dist Name	Retention Time (min)	% Area	% Height	Mn	Mw	MP	Polydispersity
1		16.440	100.00	100.00	1287384	1406123		1.092233

CN5

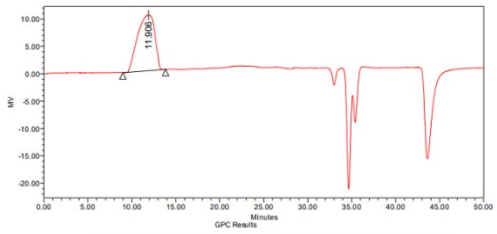

	Dist Name	Retention Time (min)	% Area	% Height	Mn	Mw	MP	Polydispersity
1		16.440	100.00	100.00	1105360	1302455		1.178309

CN7

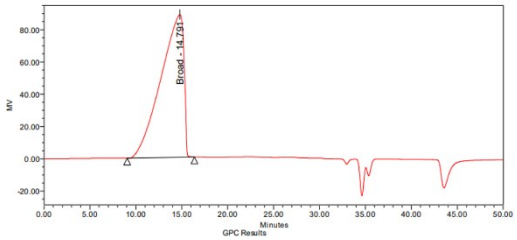

	Dist Name	Retention Time (min)	% Area	% Height	Mn	Mw	MP	Polydispersity
1		16.440	100.00	100.00	1213462	1331738		1.097470

CN9

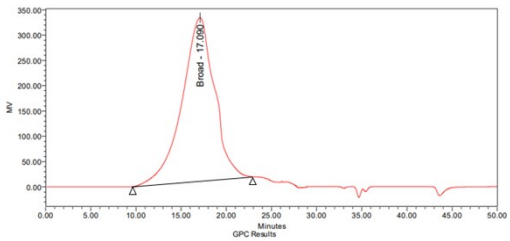

	Dist Name	Retention Time (min)	% Area	% Height	Mn	Mw	MP	Polydispersity
1		16.440	100.00	100.00	748522	1282015		1.712727

Fig. S6. Gel permeation chromatography data of the CN series copolymers.

Table S1. Summary of the optical and electrochemical properties of the neat CN series films.

Copolymers	$\lambda_{max,\ film,\ 300\ ^{\circ}C}$ [nm]	λ_{onset} [nm]	$E_{g,\ opt.}$ [eV]	HOMO[a] [eV]	LUMO[b] [eV]
CN1	792	989	1.25	-5.21	-3.96
CN3	792	978	1.27	-5.26	-3.99
CN5	800	997	1.24	-5.29	-4.05
CN7	811	993	1.25	-5.30	-4.05
CN9	817	990	1.25	-5.31	-4.06

[a] The highest occupied molecular orbital (HOMO) level was determined using the oxidation onset potential in the cyclic voltammetry (CV) measurements.
[b] The lowest unoccupied molecular orbital (LUMO) level was estimated using the $E_{g,\ opt.}$ and HOMO level.

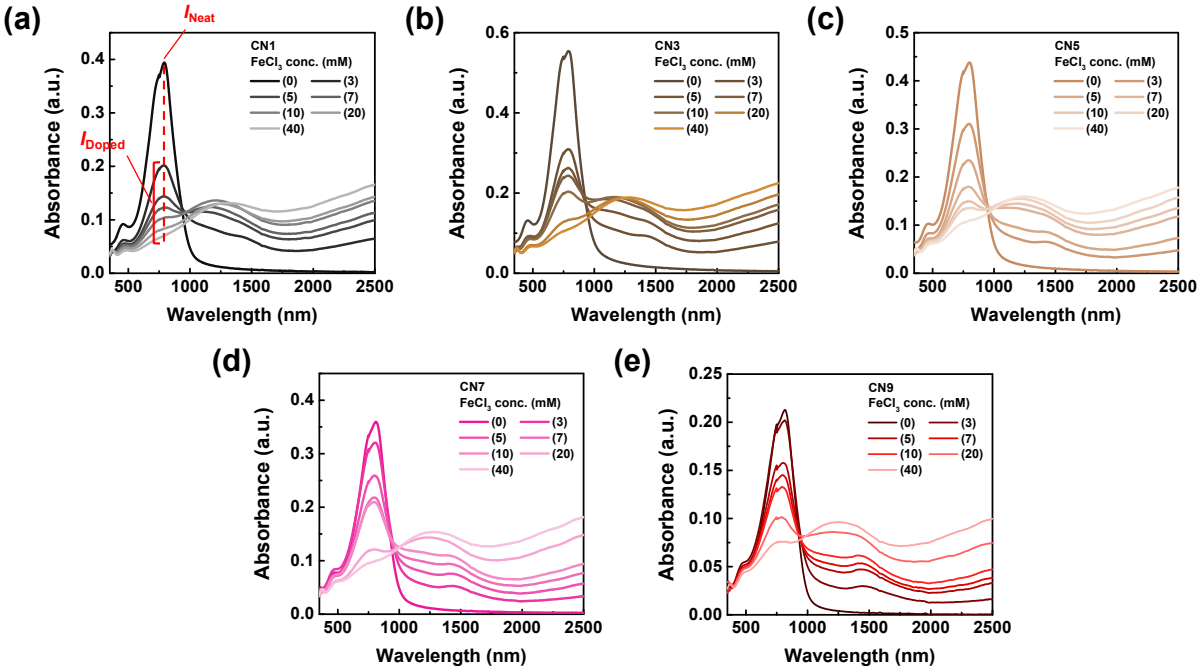

Fig. S7. UV–vis–NIR absorption spectra of the neat (0 mM) and $FeCl_3$-doped CN series films (3–40 mM). (a) CN1, (b) CN3, (c) CN5, (d) CN7, and (e) CN9.

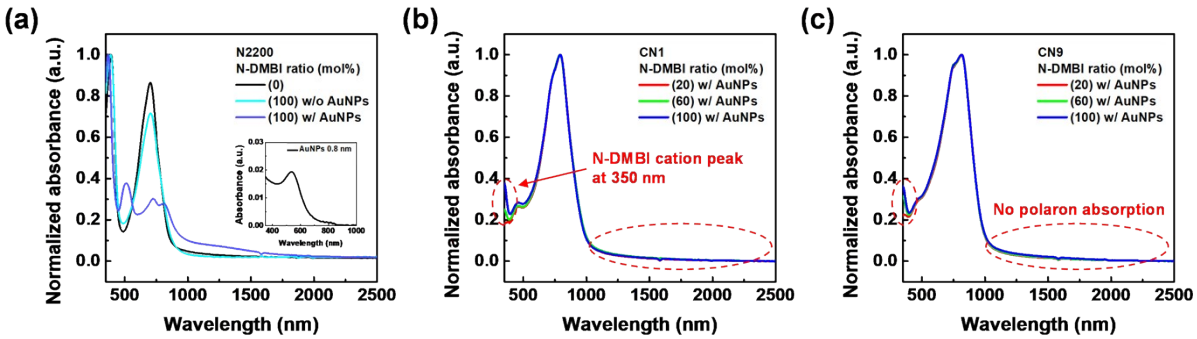

Fig. S8. UV–vis–NIR absorption spectra of the N-DMBI-doped CP films with gold nanoparticles (AuNPs). (a) N2200 (0 and 100 mol%), (b) CN1 (20, 60, and 100 mol%), and (c) CN9 (20, 60, and 100 mol%).

AuNPs were fabricated by the thermal evaporation of a gold source on glass substrates with a nominal thickness of 0.8 nm. The glass substrate with a 0.8 nm-thick AuNP layer exhibited UV–vis–NIR absorption spectra similar to those in a previous study.[4] The conjugated polymers (CPs) (N2200, CN1, and CN9) and N-DMBI were dissolved in chloroform at concentrations of 5 and 10 mg mL^{-1}, respectively, and then the CP and N-DMBI solutions were mixed to the desired N-DMBI molar ratio. The mixed solutions were spin-coated at 1500 rpm for 15 s and then annealed for 10 s at 120 °C. N2200 was successfully doped with AuNP-catalyzed N-DMBI; however, CN1 and CN9 did not exhibit polaron absorption peaks despite of the presence of an N-DMBI cation peak at 350 nm.

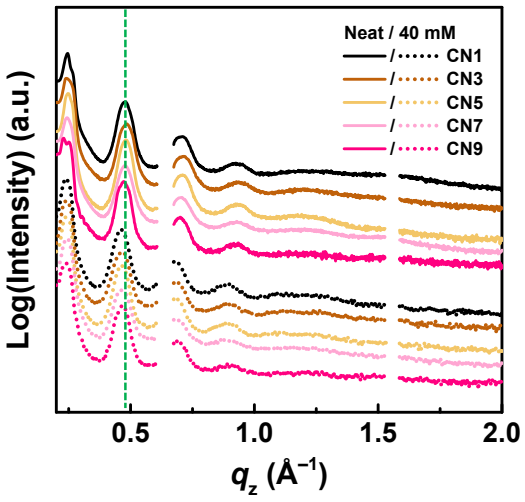

Fig. S9. Cross-sectional intensity profiles along the out-of-plane direction of the 2D-GIXD patterns of the neat and 40 mM $FeCl_3$-doped CN series films.

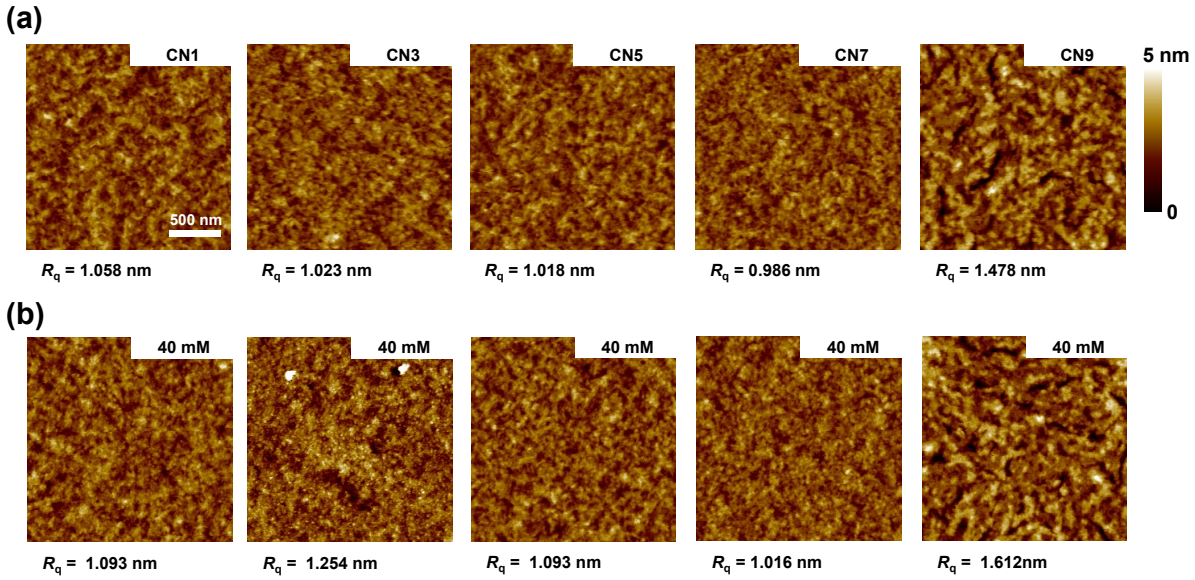

Fig. S10. Surface morphologies of the CN series films. AFM topographic images of (a) the neat and (b) 40 mM $FeCl_3$-doped films. The *R*q values are detailed below the images. All images are represented using scale bars.

Table S2. Film thickness of the neat and CN series films doped with various $FeCl_3$ concentrations (3–40 mM).

$FeCl_3$ concentration [mM]	Film thickness [nm]				
	CN1	CN3	CN5	CN7	CN9
Neat	37.5 ±2.3	56.7 ±3.0	48.4 ±2.0	43.8 ±2.7	31.8 ±5.0
3	38.5±3.8	57.1 ±2.8	48.5 ±4.1	46.7 ±6.8	32.7 ±2.9
5	36.1 ±3.3	56.6 ±3.3	44.8 ±4.3	43.2 ±3.0	29.5 ±2.6
7	39.6 ±4.3	63.6 ±3.2	46.0 ±5.2	43.2 ±1.5	33.5 ±1.4
10	38.4 ±3.6	62.6 ±2.9	44.5 ±3.0	48.0 ±4.5	31.5 ±4.0
20	40.7 ±1.4	54.2 ±1.5	48.9 ±1.4	41.1 ±2.3	30.7 ±4.4
40	36.9 ±2.2	61.5 ±4.2	54.8 ±3.3	46.2 ±1.6	35.2 ±2.9

Table S3. Thermoelectric properties of the CN series films with doped various $FeCl_3$ concentrations (3–40 mM).

	$FeCl_3$ concentration [mM]	σ [S cm^{-1}]	S [μV K^{-1}]	PF [μW m^{-1} K^{-2}]
CN1	3	7.97 ±1.43	187 ±3	27.6 ±9.6
	5	52.4 ±4.9	118 ±4	73.2 ±6.7
	7	80.9 ±7.2	90.6 ±5.1	66.4 ±5.9
	10	138.5 ±8.1	62.2 ±2.2	53.5 ±3.1
	20	170.5 ±14.5	38.5 ±0.3	25.3 ±2.1
	40	233.3 ±14.2	20.5 ±1.3	9.8 ±1.2
CN3	3	3.80 ±1.71	200 ±34	15.3 ±6.9
	5	22.4 ±2.8	160 ±3	57.1 ±7.2
	7	40.7 ±4.6	116 ±1	55.1 ±6.2
	10	68.1 ±10.3	91.8 ±3.8	57.3 ±8.7
	20	148.5 ±4.9	40.7 ±3.7	24.6 ±0.8
	40	152.9 ±10.2	21.7 ±1.1	7.2 ±0.5
CN5	3	0.62 ±0.22	334 ±4	6.9 ±2.4
	5	7.62 ±1.24	214 ±17	34.9 ±5.7
	7	37.1 ±2.9	121 ±1	54.0 ±4.2
	10	61.9 ±5.9	94.0 ±2.5	54.6 ±5.2
	20	76.8 ±3.4	57.8 ±2.6	25.7 ±0.9
	40	91.4 ±2.7	23.4 ±0.5	5.00 ±0.15
CN7	3	0.18 ±0.09	473 ±20	3.92 ±2.09

	5	3.48 ±0.62	200 ±19	13.9 ±2.5
	7	6.87 ±1.15	178 ±8	21.8 ±3.6
	10	12.9 ±2.2	152 ±3	29.6 ±5.0
	20	45.0 ±5.4	58.8 ±1.7	15.5 ±1.9
	40	71.5 ±15.5	24.7 ±0.9	4.4 ±0.9
CN9	3	0.06 ±0.03	503 ±68	1.46 ±0.81
	5	0.47 ±0.40	313 ±27	4.56 ±3.91
	7	0.91 ±0.65	292 ±1	7.78 ±5.51
	10	3.69 ±0.57	154 ±5	8.78 ±1.34
	20	13.7 ±0.7	85.5 ±0.3	10.0 ±0.5
	40	23.3 ±4.9	37.4 ±1.3	3.26 ±0.69

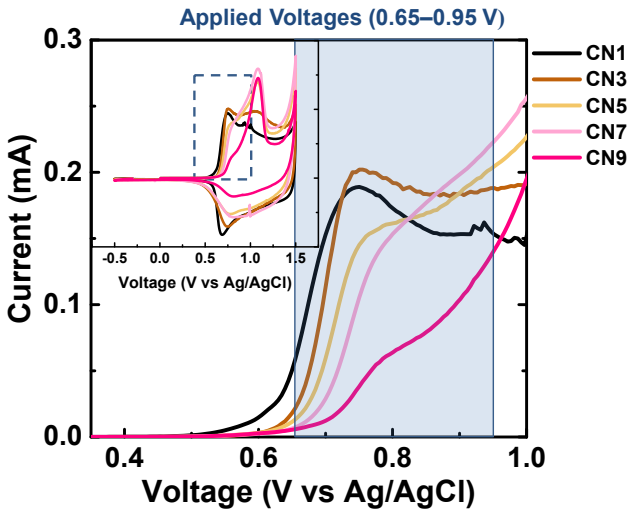

Fig. S11. Cyclic voltammograms of the CN series films coated on indium-tin oxide/glass substrates. Applied voltages of 0.65–0.95 V were used for the chronoamperometry-integrated UV–vis–NIR method.

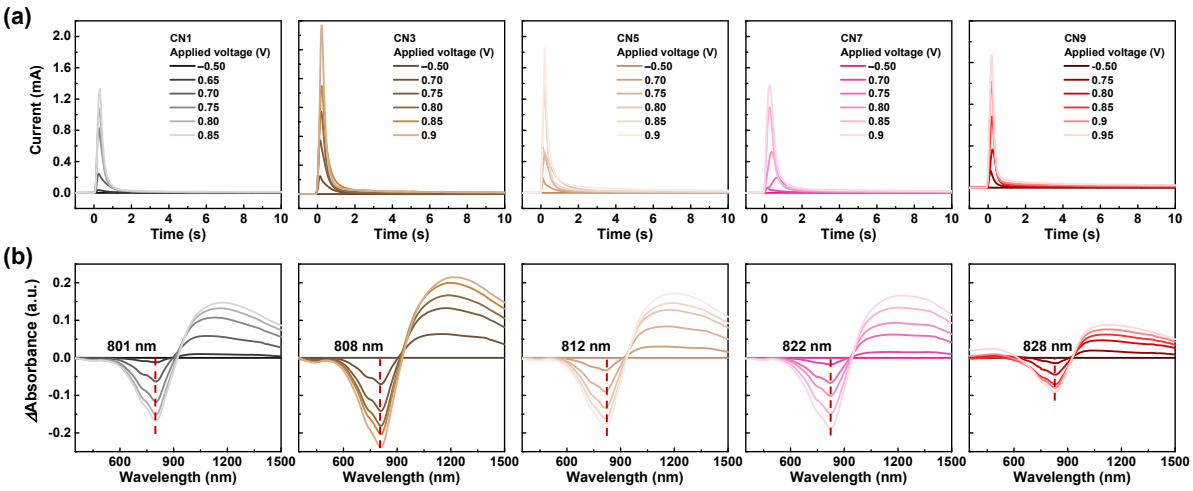

Fig. S12. (a) Chronoamperometry and (b) UV–vis–NIR absorption spectra of the CN series films at different applied voltages. The applied voltage ranges were determined from the cyclic voltammograms.

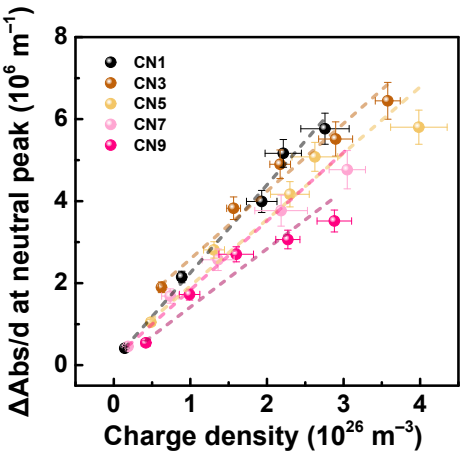

Fig. S13. Plots of the thickness-normalized absorbance difference versus charge density of the CN series films. The charge density values were extracted from the chronoamperometry results by integrating the current over time.

The chronoamperometry-integrated UV–vis–NIR spectra provided meaningful information on the charge carrier density of the $FeCl_3$-doped CN series films. First, the oxidation potentials of the polymer films were confirmed by CV measurements of the CN series films coated on ITO glass substrates (Fig. S5). Chronoamperograms were recorded while voltage was applied to the films to electrochemically oxidize the CN1–9 films (Fig. S6a). The charge densities were estimated from the total number of charges ($Q = \int_{t=0}^{\infty} I(t)dt$) and volume of the CN series films. Subsequently, the UV–vis–NIR spectra of the oxidized films were measured to obtain the absorbance difference at the neutral peak positions (ΔAbs) (Fig. S6b). The absorbance at the neutral peak position decreased after oxidation of the polymer films, and it was assumed that the absorbance difference between the doped and neat films was proportional to the charge density of the oxidized polymer films according to the Beer–Lambert law. Figure S7 shows the linear empirical relations of the thickness-normalized ΔAbs (ΔAbs/d) and charge density of the

CN series films. The thickness-normalized ΔAbs of the $FeCl_3$-doped CN1–9 films ($\Delta Abs^{Opt.}/d$) were extracted from Fig. S1. Finally, the charge densities of the $FeCl_3$-doped CN series films ($N^{Opt.}$) could be estimated from the $\Delta Abs^{Opt.}/d$ and the linear relationship shown in Fig. S7.

Table S4. Thickness-normalized absorbance difference ($\Delta Abs^{Opt.}/d$) at the neutral polymer peak position and charge density ($N^{Opt.}$) for various $FeCl_3$ concentrations.

		CN1	CN3	CN5	CN7	CN9
3 mM	$\Delta Abs^{Opt.}/d$ [10^6 m^{-1}]	5.13 ±0.32	4.32 ±0.23	2.64 ±0.11	0.90 ±0.06	0.34 ±0.05
	$N^{Opt.}$ [10^{26} m^{-3}]	2.34 ±0.15	2.04 ±0.11	1.44 ±0.06	0.44 ±0.03	0.24 ±0.04
	μ [cm^2 V^{-1} s^{-1}]	0.21 ±0.07	0.12 ±0.05	0.03 ±0.01	0.02 ±0.01	0.01 ±0.01
5 mM	$\Delta Abs^{Opt.}/d$ [10^6 m^{-1}]	6.67 ±0.41	5.15 ±0.28	4.21 ±0.17	2.32 ±0.14	1.76 ±0.28
	$N^{Opt.}$ [10^{26} m^{-3}]	3.06 ±0.19	2.55 ±0.14	2.41 ±0.10	1.29 ±0.08	1.24 ±0.20
	μ [cm^2 V^{-1} s^{-1}]	1.07 ±0.10	0.55 ±0.07	0.20 ±0.03	0.17±0.03	0.02 ±0.02
7 mM	$\Delta Abs^{Opt.}/d$ [10^6 m^{-1}]	7.23 ±0.45	5.48 ±0.30	5.35 ±0.22	3.25 ±0.20	2.19 ±0.35
	$N^{Opt.}$ [10^{26} m^{-3}]	3.32 ±0.21	2.75 ±0.15	3.11 ±0.13	1.84 ±0.11	1.54 ±0.24
	μ [cm^2 V^{-1} s^{-1}]	1.52 ±0.14	0.92 ±0.1.	0.74 ±0.06	0.23 ±0.04	0.04 ±0.03
10 mM	$\Delta Abs^{Opt.}/d$ [10^6 m^{-1}]	7.74 ±0.48	6.19 ±0.33	5.97 ±0.24	3.46 ±0.21	2.58 ±0.41
	$N^{Opt.}$ [10^{26} m^{-}	3.56 ±0.22	3.18 ±0.17	3.50 ±0.14	1.97 ±0.12	1.82 ±0.29

	^{3}]					
	μ [cm^2 V^{-1} s^{-1}]	2.43 ±0.14	1.34 ±0.20	1.10 ±0.11	0.41 ±0.07	0.13 ±0.02
20 mM	ΔAbs$^{Opt.}$/d [10^6 m^{-1}]	8.28 ±0.51	7.43 ±0.40	6.25 ±0.26	5.45 ±0.33	3.57 ±0.56
	$N^{Opt.}$ [10^{26} m^{-3}]	3.81 ±0.24	3.93 ±0.21	3.67 ±0.15	3.16 ±0.19	2.52 ±0.39
	μ [cm^2 V^{-1} s^{-1}]	2.79 ±0.24	2.36 ±0.08	1.31 ±0.06	0.89 ±0.11	0.34 ±0.02
40 mM	ΔAbs$^{Opt.}$/d [10^6 m^{-1}]	8.63 ±0.53	7.83 ±0.42	6.80 ±0.28	5.94 ±0.36	4.30 ±0.68
	$N^{Opt.}$ [10^{26} m^{-3}]	3.98 ±0.25	4.18 ±0.22	4.01 ±0.16	3.45 ±0.21	3.03 ±0.48
	μ [cm^2 V^{-1} s^{-1}]	3.66 ±0.44	2.29 ±0.15	1.42 ±0.04	1.29 ±0.28	0.48 ±0.10

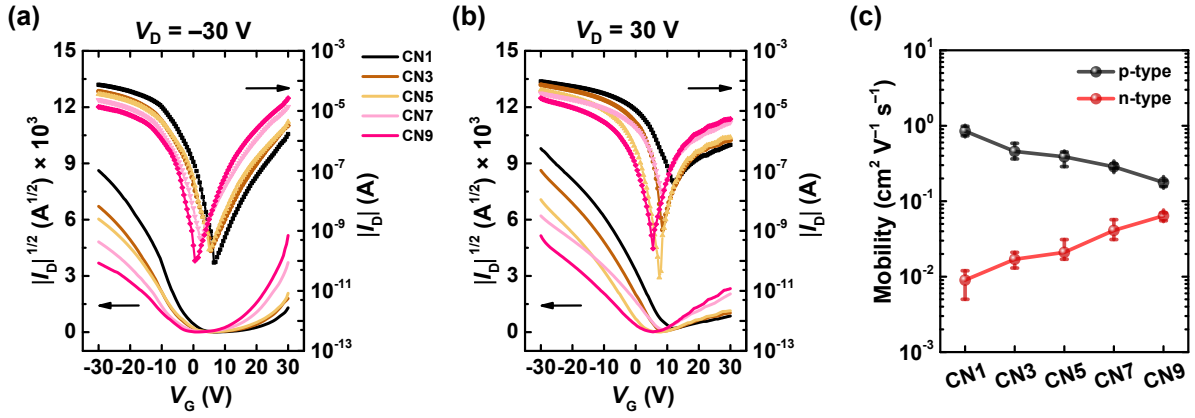

+

Fig. S14. Transfer curve of the neat CN series films. (a) V_D = –30 V and (b) V_D = 30 V. (c) P- and n-type field-effect mobilities of the neat CN series films.

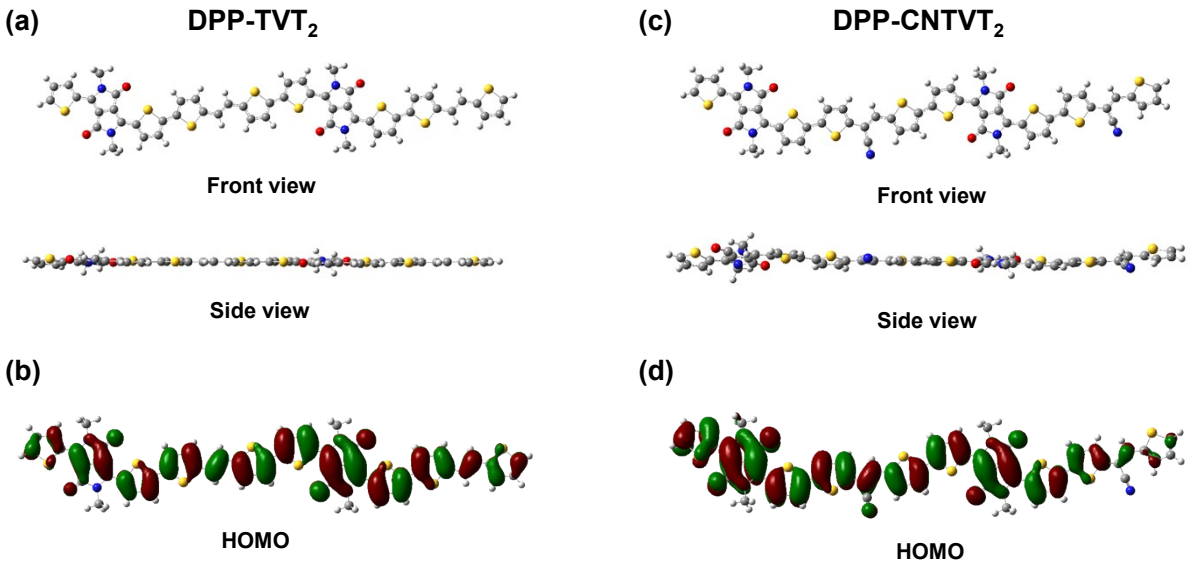

Fig. S15. Density functional theory (DFT)-optimized geometry of the neutral (Q = 0) (a) DPP-TVT_2 and (c) DPP-$CNTVT_2$ (front- (top) and side-view (bottom)). The molecular orbital (HOMO) of (b) DPP-TVT_2 and (d) DPP-$CNTVT_2$.

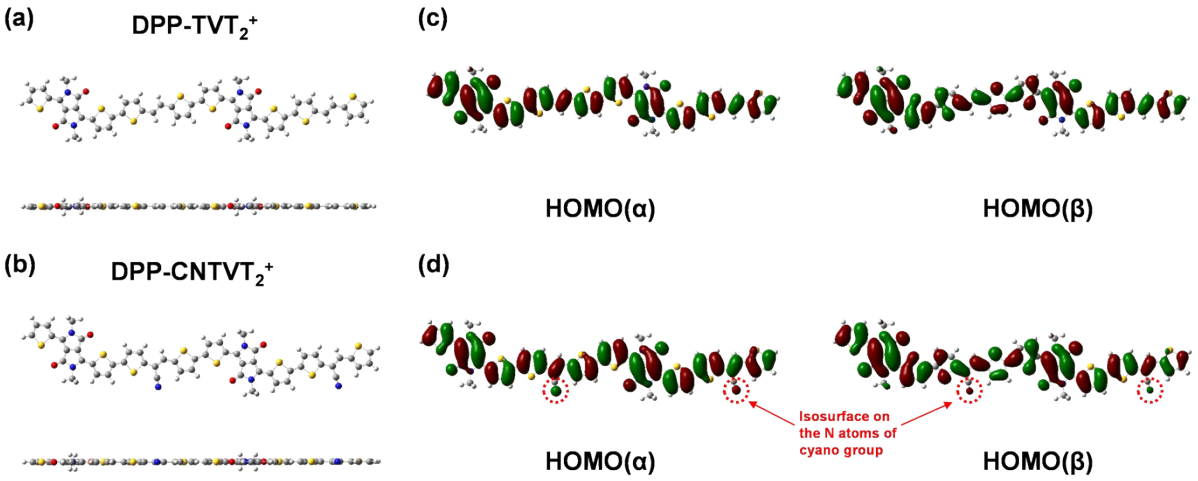

Fig. S16. DFT-optimized geometry of (a) DPP-TVT_2^+ and (b) DPP-$CNTVT_2^+$ (front- (top) and side-view (bottom)). Molecular orbital isosurface plots of HOMO(α) and HOMO(β) of (c) DPP-TVT_2^+ and (d) DPP-$CNTVT_2^+$ (α and β denote the up and down spin, respectively).

References

1 Kang, H. J. Yun, D. S. Chung, S. K. Kwon and Y. H. Kim, *J. Am. Chem. Soc.*, 2013, **135**, 14896–14899.

2 H. Chen, Y. Guo, G. Yu, Y. Zhao, J. Zhang, D. Gao, H. Liu and Y. Liu, *Adv. Mater.*, 2012, **24**, 4618–4622.

3 H. J. Yun, S. J. Kang, Y. Xu, S. O. Kim, Y. H. Kim, Y. Y. Noh and S. K. Kwon, *Adv. Mater.*, 2014, **26**, 7300–7307.

4 H. Guo, C. Y. Yang, X. Zhang, A. Motta, K. Feng, Y. Xia, Y. Shi, Z. Wu, K. Yang, J. Chen, Q. Liao, Y. Tang, H. Sun, H. Y. Woo, S. Fabiano, A. Facchetti and X. Guo, *Nature*, 2021, **599**, 67–73.